PNAS RESEARCH ARTICLE | ECOLOGY

Linking physiology, epidemiology, and demography: Understanding how lianas outcompete trees in a changing world

Hannes P. T. De Deurwaerder[a,1], Matteo Detto[a,b], Marco D. Visser[c], Stefan Schnitzer[b,d], and Stephen W. Pacala[a]

Affiliations are included on p. 11.

Edited by Donald Ort, University of Illinois at Urbana Champaign, Urbana, IL; received November 6, 2023; accepted June 24, 2024

Extending and safeguarding tropical forest ecosystems is critical for combating climate change and biodiversity loss. One of its constituents, lianas, is spreading and increasing in abundance on a global scale. This is particularly concerning as lianas negatively impact forests' carbon fluxes, dynamics, and overall resilience, potentially exacerbating both crises. While possibly linked to climate-change-induced atmospheric CO_2 elevation and drought intensification, the reasons behind their increasing abundance remain elusive. Prior research shows distinct physiological differences between lianas and trees, but it is unclear whether these differences confer a demographic advantage to lianas with climate change. Guided by extensive datasets collected in Panamanian tropical forests, we developed a tractable model integrating physiology, demography, and epidemiology. Our findings suggest that CO_2 fertilization, a climate change factor promoting forest productivity, gives lianas a demographic advantage. Conversely, factors such as extreme drought generally cause a decrease in liana prevalence. Such a decline in liana prevalence is expected from a physiological point of view because lianas have drought-sensitive traits. However, our analysis underscores the importance of not exclusively relying on physiological processes, as interactions with demographic mechanisms (i.e., the forest structure) can contrast these expectations, causing an increase in lianas with drought. Similarly, our results emphasize that identical physiological responses between lianas and trees still lead to liana increase. Even if lianas exhibit collinear but weaker responses in their performance compared to trees, a temporary liana prevalence increase might manifest driven by the faster response time of lianas imposed by their distinct life-history strategies than trees.

Barro Colorado Island | climate change | CO_2 fertilization | life-history strategies | transient dynamics

Significance

The striking increase in liana (woody vine) abundance in tropical forests is concerning from a climate change perspective. Lianas lower the carbon storage capacity of forests and hence their mitigation potential. Notably, the drivers of this widespread liana increase remain unknown. Due to the complex interaction dynamics and differing life-history strategies of lianas and trees, a multidisciplinary framework uniting physiology and forest demography is necessary to further our understanding of liana and forest dynamics. Here, we introduce a modeling framework built on extensive physiological and demographic observations collected in Panamanian tropical forests. Our analysis suggests that climate change factors promoting forest productivity, such as CO_2 fertilization, stimulate liana proliferation.

The widespread increase of Neotropical lianas (woody vines) during the last decades (1, 2) presents a striking example of compositional and structural ecosystem shifts, with a potential for far-reaching impacts. The increase in lianas may exacerbate climate change (1) by decreasing forest biomass and carbon sequestration (3), either by reducing tree growth and survival (4, 5) or by prolonging arrested succession of forest gaps (6). Currently, the underlying drivers of liana proliferation are poorly understood (7), making it difficult to predict changes in the composition and structure of forests, to discern whether these changes are of a perpetual or transient nature, and leaving open the possibility of compensating mechanisms that would protect forest carbon storage and other ecosystem functions.

The current most prominent hypotheses for liana proliferation, summarized in Fig. 1, can be grouped into four categories: CO_2 or nutrient fertilization, defaunation, drought intensification, and higher rates of natural and anthropogenic disturbance (1, 8). To understand what factors drive liana proliferation, an increasing number of studies search for the signature of changing environmental factors on growth-form-specific *performance* (e.g., responses in vital rates: growth, survival, and reproduction) and the identification of the physiological traits that may underlie such differences (9–11). However, even if the physiological mechanisms that would increase liana performance were identified, it is not clear whether they would translate into demographic advantages for lianas, especially given the dramatic differences between tree and liana life-history and resource allocation strategies (12).

The prognostic assessment of trends in liana increase does not exclusively rely on liana performance relative to trees but also depends on the interactions between lianas and their tree hosts. For example, as an increase in the force of infection enhances the spread of infectious diseases, environmental changes that induce a positive physiological response to lianas might directly promote their *infestation force* (the rate at which lianas reach and cover liana-free canopy area with leaves) and colonization ability. This direct effect on the infestation force is independent of the tree's physiological response. However, such environmental change may also stimulate a positive response in trees, resulting in faster growth

Author contributions: H.P.T.D.D., M.D., and S.W.P. designed research; H.P.T.D.D. and M.D. performed research; H.P.T.D.D. and M.D. analyzed data; H.P.T.D.D. developed and implemented the model; M.D. developed and implemented the model and provided essential empirical data for model benchmarking and validation; M.D.V. and S.S. provided theoretical suggestion for the model development and essential empirical data for model benchmarking and validation; S.W.P. provided theoretical suggestion for the model development; and H.P.T.D.D., M.D., M.D.V., S.S., and S.W.P. wrote the paper.

The authors declare no competing interest.

This article is a PNAS Direct Submission.

[1]To whom correspondence may be addressed. Email: Hannes_De_Deurwaerder@hotmail.com.

This article contains supporting information online at https://www.pnas.org/lookup/suppl/doi:10.1073/pnas.2319487121/-/DCSupplemental.

Published August 12, 2024.

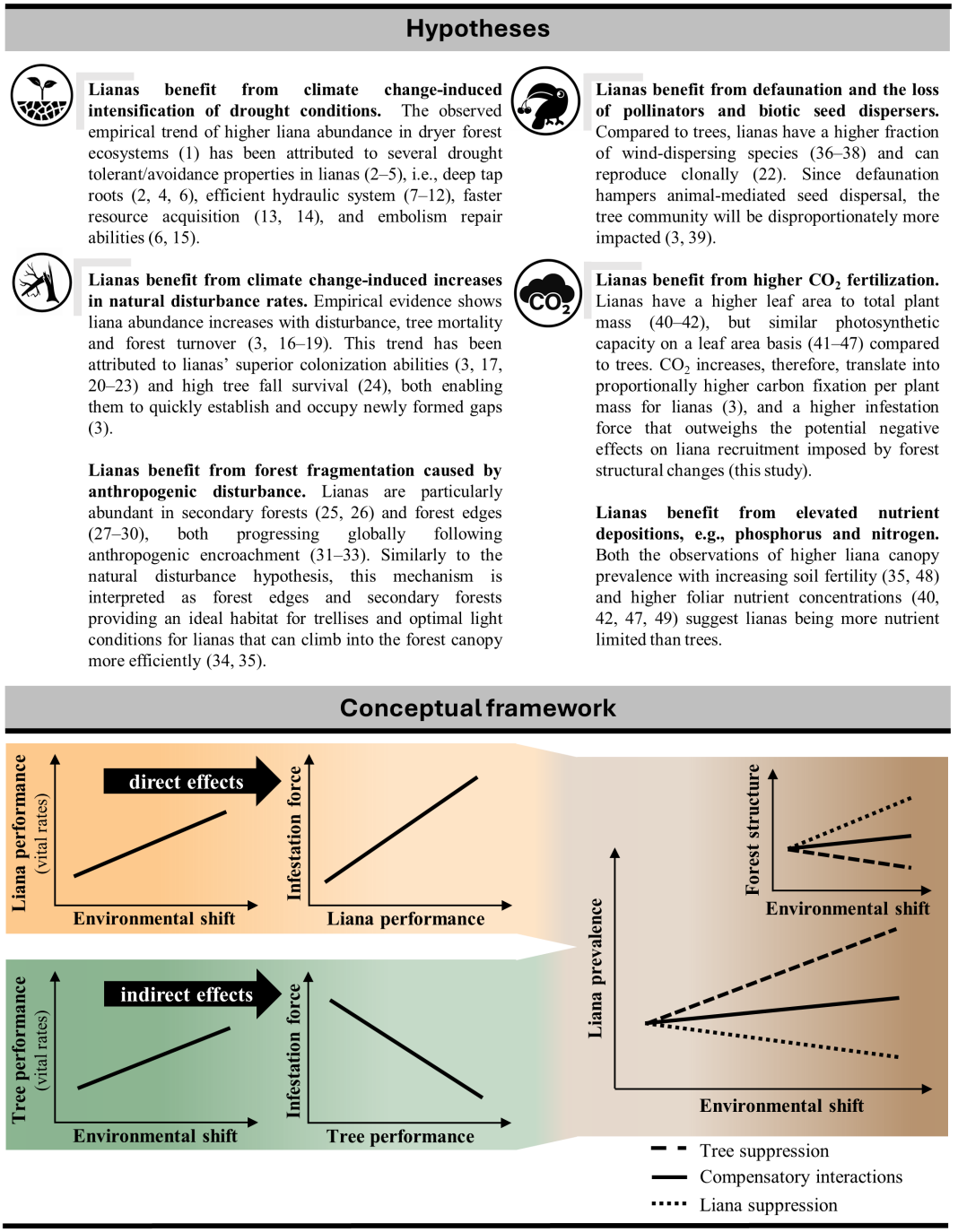

Fig. 1. The *Upper* panel shows the currently most prominent liana proliferation hypotheses, complemented by their supporting empirical trends and/or assumed underlying mechanisms. Corresponding references are listed in *SI Appendix, Appendix A*. The *Lower* panel highlights the necessity of a conceptual framework that reconciles physiological and demographic responses to assess these liana proliferation hypotheses. Specifically, an environmental shift resulting in unidirectional increases in liana and tree *performance* (e.g., growth, survival, and reproduction) can support various trends in liana prevalence (the fraction of canopy area occupied by liana leaves). This disparity in liana prevalence responses emerges from the antagonistic interactions between changes in *forest structure* (tree density, canopy height, and canopy architecture) and in *infestation force* (the rate at which lianas reach and cover liana-free canopy area with leaves). On the one hand, changes in forest structure are directly governed by tree performance, and by the imposed negative impact of lianas on tree growth and mortality. On the other hand, changes in infestation force are directly governed by liana performance, and impacted by the tree community's ability to cater toward larger tree sizes which are more difficult to colonize, and thus indirectly suppress liana infestation. Depending on whether the overall dominant force is constituted by lianas, trees, or both will drive the system towards a trend of tree suppression, liana suppression, or compensatory interactions, respectively. A more detailed description of this conceptual framework is provided in the introduction and in the *Conceptual Framework* section of the results.

and a subsequent shift in *forest structure* (e.g., tree density, canopy height, and canopy architecture) toward taller or denser forests, or both. Because lianas recruit more favorably and reach the canopy more easily in more open and shorter forests (13–16), increasing forest height and thickness could indirectly restrain liana infestation. This mechanism has been proposed to explain the relatively high abundance of lianas in seasonally dry tropical forests and the low abundance of lianas in aseasonal wet forests (17–19).

Fig. 1 shows how antagonistic mechanisms—the direct effect on the infestation force and the indirect effect on forest structure—can stimulate, compensate, or suppress liana proliferation. An environmental shift causing a positive response to liana performance will stimulate liana *canopy prevalence* (e.g., the fraction of canopy area occupied by liana leaves) by increasing the infestation force. The liana increase will negatively impact trees by suppressing growth and increasing mortality. If this effect is stronger than the positive effect of the environmental change on tree performance, forest structure will be suppressed (tree suppression, dashed lines). Having the ability to suppress forest structure and biomass despite increased tree growth rates is the most concerning scenario for the global impact of lianas on forest carbon stocks. Contrarily, if the positive effect of the environmental change on trees compensates for the negative effect imposed by lianas, forest structure can still increase moderately and, indirectly, reduce the severity of liana proliferation (compensatory interactions, solid lines). Finally, if the increase in forest structure is strong enough to suppress liana recruitment and access to the canopy, liana abundance can decrease despite the physiological boost to liana performance (liana suppression, dotted lines).

The case where environmental shifts cause opposing performance responses for lianas and trees will naturally lead to a demographic advantage of the positively stimulated growth form while suppressing the other growth form. However, this scenario is probably of

little interest for many environmental shifts under consideration, as they often produce unidirectional responses for lianas and trees, albeit of different magnitude. For example, CO_2 fertilization increases growth for both lianas and trees (20, 21). Similarly, drought intensification increases mortality for both growth forms (22).

Theoretical models can help disentangle the complex interplay between physiological responses and demographic interactions. For example, host-parasite models have been used to explore analytically the ecological principles of how demography shapes liana abundance (23, 24). However, these models do not explicitly represent forest structure nor consider the physiological responses to changing environmental factors. On the other side of the spectrum, lianas have recently been incorporated into dynamic vegetation models (25, 26), allowing mechanistic representation of the effects of environmental drivers and the physical interactions between lianas and trees. While these models are critical to quantify the impact of lianas on the terrestrial carbon cycle, they are complex and analytically intractable, making it difficult to systematically explore the basic principles and disentangle the fundamental processes that lead to liana proliferation under different scenarios.

In this study, we develop a minimalistic model with the complexity necessary to encompass alternative hypotheses about the proliferation of lianas and their impact on trees, while retaining the simplicity necessary for analytical results and syntheses. Because most of the alternative hypotheses are based on physiological responses, the model should incorporate three fundamental components: plant physiology, resource allocation, and demography (Fig. 2). A resource allocation scheme is necessary to link the physiological response of each growth form to a demographic effect; for example, an increase in resource acquisition can result in faster growth or higher fruit production. The demographic model must represent the interactions between lianas and forest structure, making assumptions about how lianas reach their hosts and spread in the canopy.

To illustrate the proposed conceptual framework, we apply the model to study the impact of shifts in forest productivity that may result from increases in CO_2 fertilization and seasonal drought using stem diameter growth rates to measure plant performance. Growth rate is the most extensively characterized and mechanistically understood vital rate and can be modeled from basic principles of plant carbon economy (assimilation and allocation). The model is parameterized and benchmarked using physiological and demographic data. We use an extensive dataset collected in Panamanian tropical forests, including one of the largest longitudinal surveys of lianas and trees (12, 27). We show how the model provides a platform to decouple isolated responses of environmental drivers and biotic processes on the growth-form-specific physiological performance and vital rates, rendering changes in liana abundance. We monitor the temporal behavior of our system from the moment of perturbation until a new steady state is reached, i.e., transient and equilibrium conditions, respectively. The goal of our study is twofold: i) introducing a liana modeling framework that reconciles physiology, demography, and epidemiology and which supports our final goal of ii) revealing the mechanisms that lead to liana proliferation. Specifically, we evaluate whether the increase in ambient CO_2 and drought underlie observed liana abundance increases and whether such changes may be of a transient nature.

Results

Conceptual Framework. We use liana prevalence (P_L), defined as the fraction of the canopy area occupied by lianas as an indicator of liana infestation. At equilibrium, P_L can be determined by a unique combination of vital rates that form the solution of a size-structured demographic host-parasite model (*Materials and Methods*), i.e., $P_L = P_L\left(v_T, v_L\right)$, where v is a set of vital rates (e.g., growth, mortality, and fecundity) for trees, subscript T, and lianas, subscript L.

To study the impact of an environmental shift (E) on liana prevalence, we decompose changes in P_L into: i) direct impacts on liana infestation force through changes in liana physiological performance ($\frac{dv_L}{dE}$), and ii) indirect impacts of forest structure via alterations in tree physiological performance ($\frac{dv_T}{dE}$). Mathematically, this can be expressed as:

$$\underset{\substack{\Downarrow \\ \textit{change in} \\ \textit{liana prevalence}}}{\frac{dP_L}{dE}} = \underset{\substack{\Downarrow \\ \textit{direct effect of} \\ \textit{infestation force}}}{\frac{\partial P_L}{\partial v_L}\frac{dv_L}{dE}} + \underset{\substack{\Downarrow \\ \textit{indirect effect of} \\ \textit{forest structure}}}{\frac{\partial P_L}{\partial v_T}\frac{dv_T}{dE}} \quad . \qquad [1]$$

These two effects have opposite signs for an environmental shift that changes plant performance in the same direction for trees and lianas.

In this study, we focus on changes in optimal carbon gain rate (G^*), i.e., the difference between net photosynthesis and water stress cost per unit of leaf area; analogous frameworks can be formulated for other physiological functions. The model starts from the assumption that photosynthesis and metabolic costs are proportional to the crown area of a plant with full access to light. Using a power-law allometry relating crown area, a_c, to structural mass, B, i.e., $B_j = \phi_j a_c^{\theta}$ (parsimoniously assuming the same scaling exponent for lianas and trees), a simple allocation scheme shows that biomass per unit of crown area grows linearly with time (*Materials and Methods*). Thus, we chose $x = \frac{1}{\phi}\frac{B}{a_c}$ as the plant dimension that represents size in the model (for standard allometry where $B \sim D^{2.5}$ and $a_c \sim D^{1.5}$, x has the same dimension as the diameter D). With these assumptions, we can express the change in growth rate, g, as a function of an environmentally driven change in optimal carbon gain, as:

$$dg_j = \frac{\theta - 1}{\theta}\frac{1-\varphi}{\eta\phi_j} dG_j^* \quad j = L, T \qquad [2]$$

where φ and η are universal parameters representing the fraction of available carbon allocated to reproduction and the respiratory growth cost, respectively. Because part of the available carbon is allocated to reproduction, fecundity, and growth vary jointly. Combining Eqs. **1** and **2** allows us to express the conditions for liana increase, i.e., $\frac{dP_L}{dE} >> 0$, for a positive change in carbon gain of lianas and trees as:

$$\underset{i}{\frac{dG_L^*}{dG_T^*}} > \underset{ii}{-\frac{\phi_L}{\phi_T}} \underset{iii}{\frac{\partial P_L/\partial g_T}{\partial P_L/\partial g_L}} \qquad \frac{dG_T^*}{dE} > 0 \quad . \qquad [3]$$

Eq. **3** shows that the problem of identifying the mechanisms of liana proliferation encompasses three interconnected processes: i) physiological responses to an environmental shift, ii) allocation requirements, and iii) demographic (host-parasite) interactions. The inequality sign in Eq. **3** must be reversed for a negative change in carbon gain for trees $\left(\frac{dG_T^*}{dE} < 0\right)$. In that case, if lianas have a positive response, Eq. **3** is always verified.

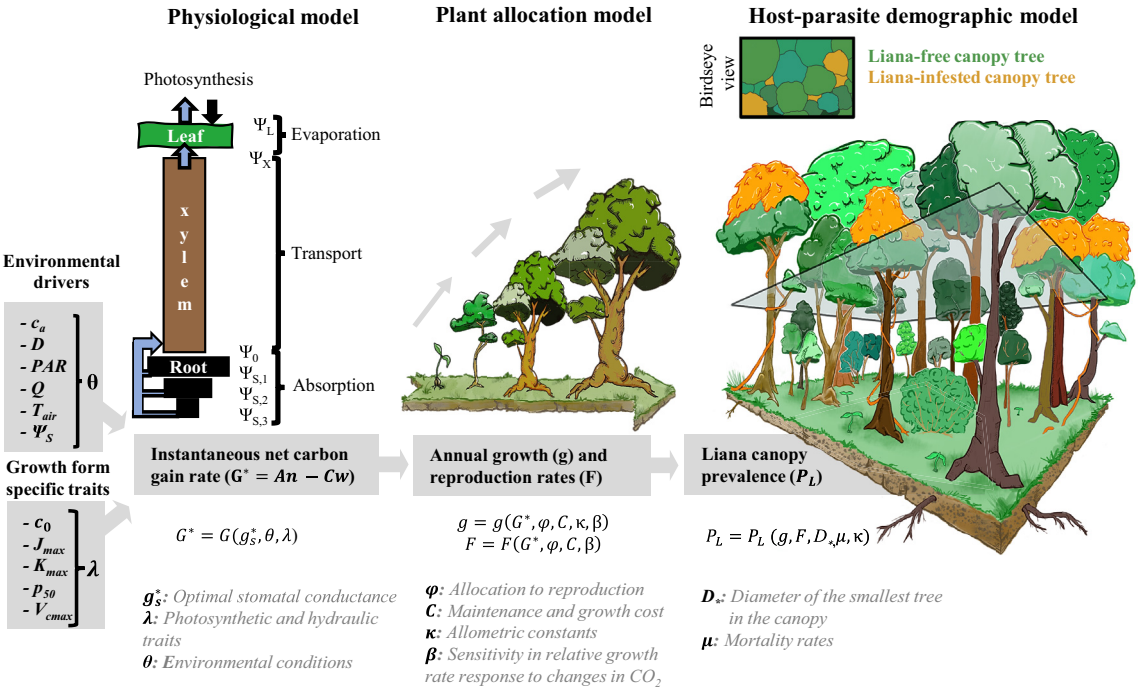

Fig. 2. Conceptual mechanistic forest model representation. The physiological module is a coupled photosynthetic-hydraulic system comprising three elements: absorbing roots, transporting organs (xylem tissue in stem, branches, and petioles), and the evaporative/photosynthetic surface of leaves. This module calculates the optimal carbon gain rate G^* as the difference between the instantaneous rate of net photosynthesis, A_N, and the cost of water stress, C_w. Environmental drivers are ambient CO_2 concentration (c_a), vapor pressure deficit (D), photoactive incoming radiation (PAR), air temperature (T_{air}), and soil water potential (Ψ_S). The model is evaluated separately for wet and dry seasons and an annual carbon budget is computed for any given dry season length (Q). For growth form-specific traits, the module requires the cost of water stress (c_0), the maximum electron transport rate (J_{max}), the maximum hydraulic conductance (K_{max}), the water potential corresponding to a 50% loss in whole plant conductance (p_{50}), and the maximum carboxylation velocity (V_{cmax}). The plant allocation module converts G^* into annual growth and reproduction rates (resp. g and F) given the allocation fraction to reproduction (φ), the growth form allometric constants (κ), the maintenance and growth respirative costs (*C*), and the sensitivity in relative growth rate response to changes in CO_2 (β). In the final step, the host-parasite demographic module uses g and F to evaluate forest structural properties such as the size abundance distribution and the size of the smallest tree in the canopy (D_*), and the fraction of infested trees from which the liana canopy prevalence (P_L) is computed. A complete description of the model, parameters, and calibration is provided in the *Materials and Methods* section and *SI Appendix, Appendix B–F*, respectively. Drawings are made by H.P.T.D.D. using the open-source painting program Krita (version 4.4.1.; www.krita.org).

Forest Structural Properties. The mean canopy occupancy index, $\overline{COI}$, (i.e., the fraction of a host's canopy occupied by lianas) observed at the Barro Colorado Island shows a unimodal pattern with host size, peaking at a 20 to 30 cm range (Fig. 3*A*, red curve). This specific size range corresponds roughly to the transition between understory and canopy layer. From observed tree size abundance distribution and crown allometry, we estimated that the average size of the smallest tree belonging to the canopy layer is D_* = 33 cm (*SI Appendix, Appendix G*). Once in the canopy layer, the $\overline{COI}$ systematically declines with tree size, indicative of a lower liana infestation success in taller trees. Interestingly, the assessment of $\overline{COI}$ of infested trees suggests higher infestation severity in deciduous than in evergreen canopy trees (Fig. 3*B*).

Several liana infestation algorithms that differ in the implementation of liana climbing and crown expansion strategies (*Material and Methods*) were evaluated (Fig. 3*A*). The model that provides the best data representation (Fig. 3*A*, full black line), and that is used for all the following analyses, was obtained by assuming the probability of lianas reaching their hosts' canopy to be proportional to D_* and that lianas have an exponential crown expansion rate. From the model perspective, only canopy lianas are considered to represent the population's reproductive individuals, thus the absence of $\overline{COI}$ in small host sizes reflects the understory lianas' disproportionately low contribution to reproduction. Analog to the empirical observation, a decaying $\overline{COI}$ trend with host size was made explicit in the host-parasite model, as the $\overline{COI}$ of host size *x* can be expressed as (from steady state Eq. **10c**):

$$\overline{COI}(x) = \frac{\lambda(x, x_*)}{\mu_c + \nu + \xi + \lambda(x, x_*)}, \quad [4]$$

where $\lambda(x, x_*)$ is the size-dependent liana infestation force, μ_c, ν, and ξ are the canopy tree mortality rate, the liana-induced lethality, and the tree shedding rate, respectively. The infestation force also depends on forest structure via an exponential decay function of x_*, representing the probability of lianas emerging from the understory layer (where x_* is the tree size corresponding to D_*, see *SI Appendix, Appendix E*).

Given the model assumptions and benchmarked for Barro Colorado Island (BCI; P_L = 0.2 and D_* = 33), the model qualitatively represents the empirical forest structure and size-specific infestation levels (Fig. 3*C*). Yet, compared to the BCI data, it overestimates the contribution of smaller-size hosts (and consequently underestimates the contribution of larger-size trees).

Case Study: Equilibrium Conditions. This case study explores conditions that may drive liana proliferation under two of the more prominent hypotheses: an increase in CO_2 concentration and dry season length. To represent all potential scenarios described in the aforementioned conceptual framework (Fig. 1), the relative growth response sensitivity of lianas and trees to an increase in CO_2 was modified from its standard ($\beta_L = \beta_T = 1$).

An increase in CO_2 stimulates plant growth (Fig. 4 *A* and *B* and *SI Appendix*, Fig. S9) and, as such, can lead to an upsurge in

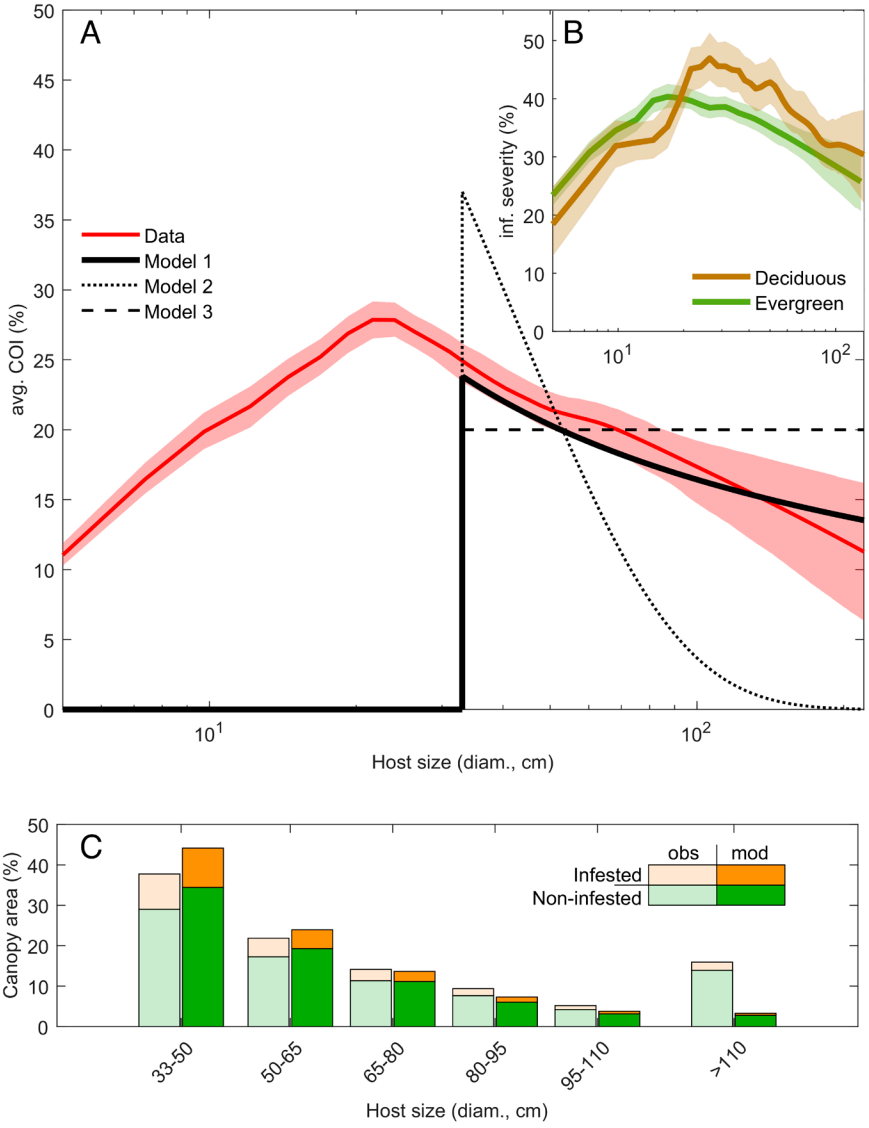

Fig. 3. (*A*) Simulated (▬) and observed (▬) average liana $\overline{COI}$; (the fraction of a host's canopy occupied by lianas) with host size. The three models assess distinct liana infestation algorithms provided in Table 1. Since understory lianas are assumed not reproductive, they are not represented in the model. (*B*) Observed liana infestation severity, i.e., the $\overline{COI}$ of infested trees, for deciduous (▬) and evergreen (▬) hosts. Empirically observed trends in panels (*A* and *B*) were computed from data obtained from ref. 23, using a smoothing averaging moving window (20%). The 95% CI (shaded areas) were computed via bootstrapping (250 iterations). (*C*) Empirical (Barro Colorado Island 50 ha census, hatched bars) and model predicted (filled bars) canopy area occupied per host size cohort. A distinction is made between liana-infested (▬) and liana-free (▬) canopy trees.

liana prevalence by amplifying the infestation force. Such an increase in liana prevalence (Fig. 4*C*) is associated with either a modest increase or a decrease in plot biomass and forest structure (Fig. 4*D*), respectively, a compensatory ($\beta_L = \beta_T$, solid) and tree-suppressing ($\beta_L \gg \beta_T$, dashed) interaction. By contrast, a liana-suppressing interaction arises when the negative impact of an increasing forest structure upon the success rate of lianas reaching the canopy overcompensates for the increased infestation force ($\beta_L \ll \beta_T$, dotted).

Extending the dry season length leads to a mutual decline in liana and tree diameter growth rates (Fig. 4 *E* and *F*) driven by a lower instantaneous rate of photosynthesis and higher cost for water stress over the dry compared to the wet season (*SI Appendix*, Fig. S8). Generally, such conditions cause a reduction in the infestation force and liana prevalence (Fig. 4 *G* and *H*). However, a scenario of a moderate increase in liana prevalence could arise, but only when the lowered forest structure induced by drought reduction in tree growth promotes liana recruitment in the canopy despite the decline in liana's growth (dotted lines in Fig. 4 *G* and *H*). To achieve a significant increase in liana prevalence in the model, the trees' relative growth response to CO_2 must, at the very least, be quadruple that of lianas—a higher sensitivity to CO_2 means a higher decline in photosynthesis with drought.

Case Study: Transient Dynamics. We used the model to explore the transient dynamics of liana prevalence in response to a gradual 50-y step increase in CO_2, resembling the natural CO_2 rise between 1975 and 2024 (from 330 to 424 ppm). We enforced a β_L optimization, i.e., the lianas' relative growth response sensitivity to an increase in CO_2, to produce no difference in liana prevalence between the initial and final timesteps of the simulation (500 y). Specifically, we targeted a scenario where the increase in infestation force is compensated exactly by the negative impact of increasing forest structure.

In the transient, the liana prevalence was temporarily increased (Fig. 5*B*). Lianas can instantly capitalize on the increase in productivity and infestation vigor, while the compensating effect of increasing forest structure (Fig. 5*C*), which limits the liana recruitment into the canopy, and only slowly catches up to cause the liana prevalence to fall back to its base level. This phenomenon is thus caused by the difference in response time between lianas, which have a faster dynamic, and trees, which have a higher inertia. Hence, any environmental driver that results in a liana relative growth rate increase will promote a temporary liana prevalence increase, independent of the relative growth response of trees. Diametrically, any reduction in liana relative growth rate will instigate a temporary reduction in liana prevalence.

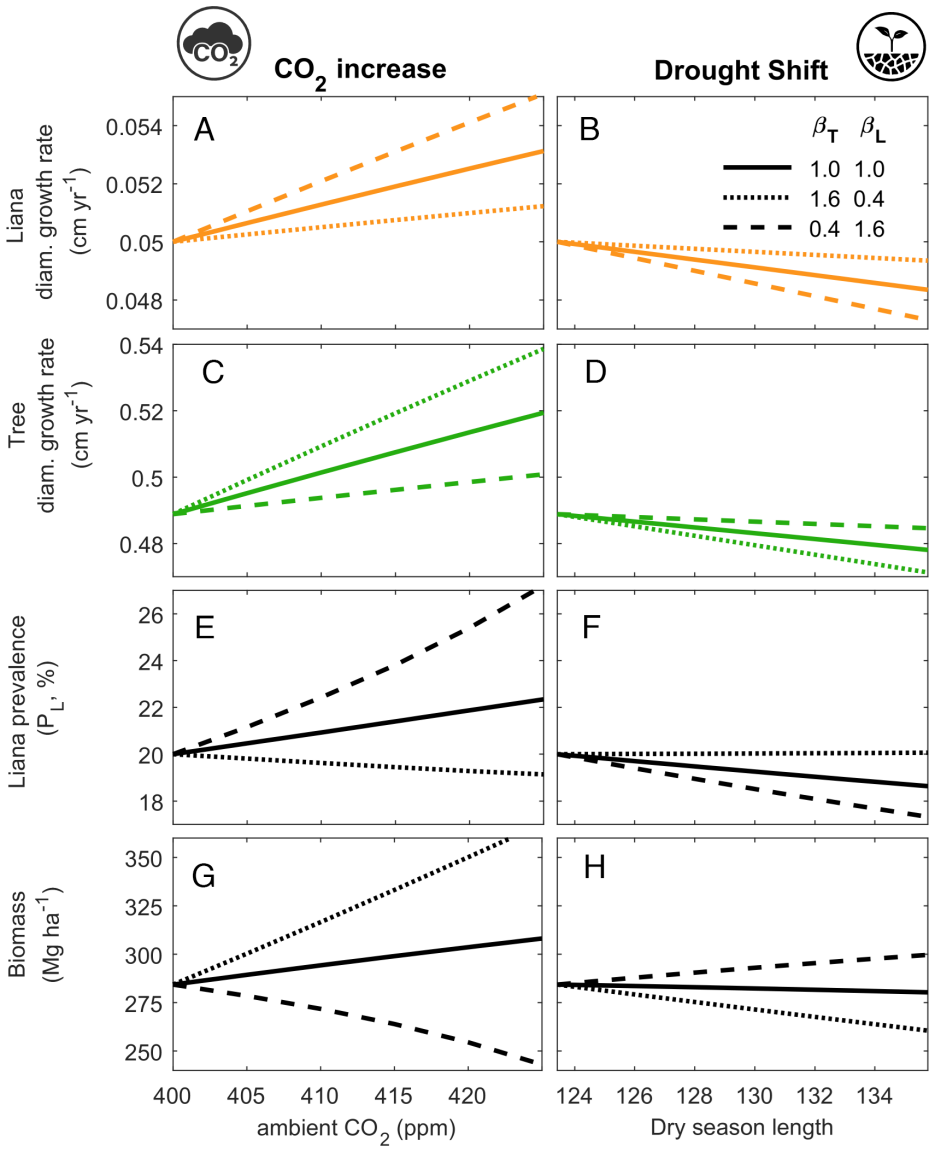

Fig. 4. Changes in the diameter growth rates of lianas (*A*, *B*) and trees (*C*, *D*), liana canopy prevalence (P_L; *E*, *F*), and plot biomass (*G*, *H*) following an increase in ambient CO_2 (CO_2 increase; *Left* panels) and in dry season length (Drought shift; *Right* panels). Each scenario explores distinct relative growth response sensitivity to an increase in CO_2 for lianas and trees (β_L and β_T, respectively), where the combinations of β_L and β_T are selected to represent all potential scenarios depicted in our conceptual framework (Fig. 1). Specifically, distinct line types indicate a scenario of compensatory interactions (solid), liana suppression (dotted), and tree suppression (dashed). Diameter growth rates represent the absolute growth for a liana and tree of 1.6 and 33 cm diameter, respectively, with initial conditions obtained from the Barro Colorado Island 50 ha plot forest surveys.

Discussion

Many studies on liana increases in tropical forests focused on identifying different physiological responses between lianas and trees to environmental stimuli (20, 21, 28–30). Our model shows that liana proliferation can develop even when physiological responses are identical in lianas and trees, emphasizing the importance of using a framework that couples physiology with life-history strategy and demography to aid the interpretation of liana increase studies.

Our model suggests that environmental drivers that increase plant productivity lead to a demographic advantage for lianas, a phenomenon attributed to two fundamental mechanisms: i) the interplay between forest structure (i.e., height and density) and infestation force (Fig. 4); and ii) response time differences between lianas and trees (Fig. 5). The first mechanism is key in driving the long-term trends (i.e., steady state) in liana prevalence. Specifically, elevated photosynthetic rate increases available carbon and translates into higher liana recruitment, climbing rate, and canopy expansion. This direct effect on infestation force positively impacts liana prevalence, independently on trees, and it is mainly mediated by liana parameters that regulate carbon allocation and allometry (*SI Appendix*, Figs. S5–S7). Similarly, trees achieve faster growth rates, which causes a taller and more dense forest structure (i.e., higher D_*) that lianas colonize. While increased dense forest structure indirectly affects lianas because a lower fraction of lianas reach the canopy and liana prevalence decreases with host size, it only partially compensates for the lianas' advantage resulting from the direct effect on infestation force. The second mechanism, i.e., the difference in response time, generates a transient dynamic on the long-term equilibrium of liana prevalence. This perturbation manifests from the much faster response time to the CO_2 increase of lianas compared to trees (31, 32). Specifically, lianas capitalize on increased productivity, boosting their infestation force and prevalence before the forest structure limits liana recruitment into the canopy (and hence the liana increase). The opposite is true for a decline in forest productivity, showing an initial rapid decline in lianas followed by a slow recovery as the positive effect of a lowered forest structure manifests. The fast pace of climate change further underscores the importance of these temporary dynamics, as such perturbations could mask the underlying long-term liana prevalence trends and might cause ecosystem instabilities (33, 34).

According to our model, CO_2 fertilization remains a plausible driver of liana proliferation and increase. Importantly, an increased liana prevalence can manifest when physiological and vital rate responses of both growth forms are identical. The lack of differential responses between lianas and trees to CO_2, as observed empirically

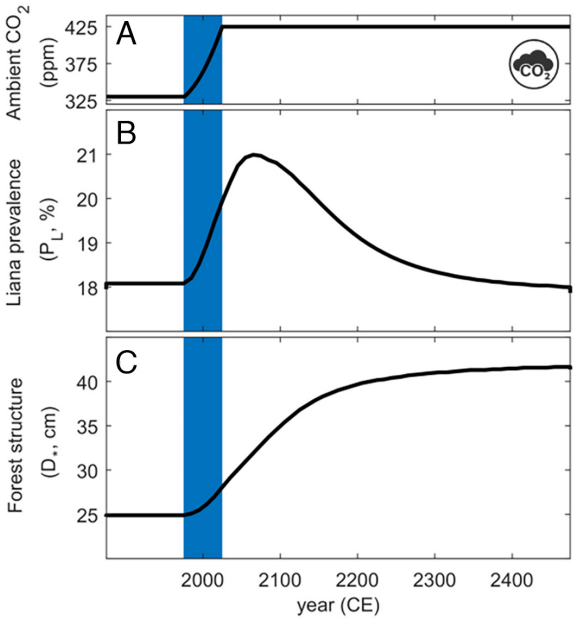

Fig. 5. Transient dynamic analyses showing how a gradual 50-year step increase in CO_2 (panel *A*) affects liana prevalence (panel *B*) and forest structure (panel *C*). This analysis imposed a β_L optimization (i.e., lianas' relative growth response sensitivity to an increase in CO_2) leading to equal liana prevalence at the start and end of the simulated period (500 y). The blue zone highlights the 50-y period of CO_2 increase (330 to 424 ppm). The size of the smallest tree belonging to the canopy layer (D_*) is used as a metric for forest structure.

(20), therefore, is not sufficient evidence to exclude CO_2 fertilization as a driver of liana proliferation.

Increases in drought conditions slow liana and tree diameter growth by dwindling net carbon gain rates, generally leading to a long-term declining trend in liana canopy prevalence in combination with a shorter-lived negative perturbation during the transient. Two mechanisms underlie the observed long-term trend. First, at the demographic level, drought has the opposite effect of CO_2 fertilization and thus reduces the infestation force. Second, at the physiological level, lianas may have higher drought sensitivity than trees. The latter observation is in line with Willson et al. (35) who found that based on the observed differences in hydraulic traits and architecture, trees should outperform lianas during increasing drought conditions, especially in forests already subjected to seasonal drought (but see refs. 36–38). Yet, our model shows that long-term increases in liana prevalence could develop if the rate of forest structure change outweighs the decline in infestation force, a condition that may manifest when lianas have a much lower drought sensitivity compared to trees.

Current observations attribute a high drought sensitivity to lianas because they are burdened with a higher risk of cavitation and a longer hydraulic pathway (39–42), increasing the whole plant's resistance to water transport (7, 35, 41, 43). The higher cavitation risk is only partially compensated by higher sapwood-specific conductivity because of the smaller sapwood-to-leaf area ratio (Huber value). However, it is possible that lianas rely on alternative—currently understudied or unknown—physiological mechanisms that buffer their drought sensitivity. For example, lianas have greater concentrations of nonstructural carbohydrates in their stems than trees (44), which may support stronger osmotic regulation to reduce the loss of turgor and increase drought tolerance (45), and allow them to recover better from drought (46). Exploration of alternative strategies for the impact of water stress, i.e., accounting for delayed and imperfect xylem recovery (47) and postdrought recovery dependence on nonstructural carbohydrates (48), may prove insightful. Additionally, including leaf phenology in response to seasonal drought, may change the trees' drought sensitivity and liana–host interactions. Since drought increases forest deciduousness (49), lianas may take advantage of the more open forest structure to recruit and climb the canopy, for example, along gap edges where they are generally more abundant (8, 50). Even at the host level, our observations show higher infestation severity in deciduous compared to evergreen trees (Fig. 4*B*) with lianas presumably capitalizing on the improved light conditions during the leaf-off period. Increased forest deciduousness could, therefore, boost liana climbing and canopy expansion rate, and might generate higher liana prevalence despite the negative impact of water stress on the overall productivity of lianas and trees. This indirect mechanism should be subject to future studies as it could also explain the observed trend of increasing liana abundance with lower rainfall (31). Our model does not simulate gap-phase dynamics, gap structure, or changes in forest deciduousness, and thus, we could not investigate this hypothesis in the current study (12).

Considering forest structure and its changes is paramount in assessing trends in liana canopy prevalence. Smaller canopy trees contribute disproportionately to liana prevalence because they are colonized faster on an individual basis (a smaller crown can be filled in less time), and they are more abundant but occupy a smaller portion of the sun-exposed forest area. By contrast, larger trees are more likely to be liana-free. Because lianas reduce the growth and increase the mortality of their host, they reduce the chance for infested trees to transition into the emergent forest layer, a phenomenon previously described as "the escape hypothesis" (51, 52). This trend is not imposed in the model, but rather, it naturally emerges from the model and generates a declining liana canopy prevalence with increasing hosts' size (Fig. 3), a general pattern that has been observed in Panamanian forests (53, 54). Moreover, the model approximates both BCIs' forest structure and liana COI despite not being calibrated against forest structure. The exponential form of the tree size distribution is driven by the lack of forest patch-level disturbance that would generate a more complex forest structure comprising patches of different ages (54).

The model successfully predicts various measured physiological drought responses of lianas and trees (Fig. 6). However, empirical observations also show a dry season growth advantage for lianas (37) and an overall low proportion of deciduousness among lianas and differing leaf phenological patterns compared to trees (55–57). Such observations are puzzling. For example, lianas having higher growth rates during the dry season is not consistent with a reduction in leaf gas exchanges, i.e., photosynthesis, which has been observed in many studies (11, 36, 58), or the decline in height growth rates (31). Reconciling plant hydraulic theory with these patterns will require coupling mechanistic models of growth and phenology at seasonal or higher temporal scales (59).

This study highlights the challenges in analyzing liana prevalence due to transient factors that are hard to identify in existing datasets. Despite utilizing data from BCI, which includes one of the most comprehensive and longest-running liana surveys, our efforts to implement models and test hypotheses faced hurdles due to data scarcity and conflicting information. One underexplored area is the timing of liana emergence and expansion in the canopy, and the factors limiting their ability to colonize hosts, such as host height, leaf habit, and competition with other lianas. Sensitivity analysis emphasized the importance of accurately characterizing liana allometry for understanding biomass accumulation and growth (*SI Appendix*, Figs. S5–S7). Our understanding of the prolonged impacts of lianas on forest carbon would benefit from

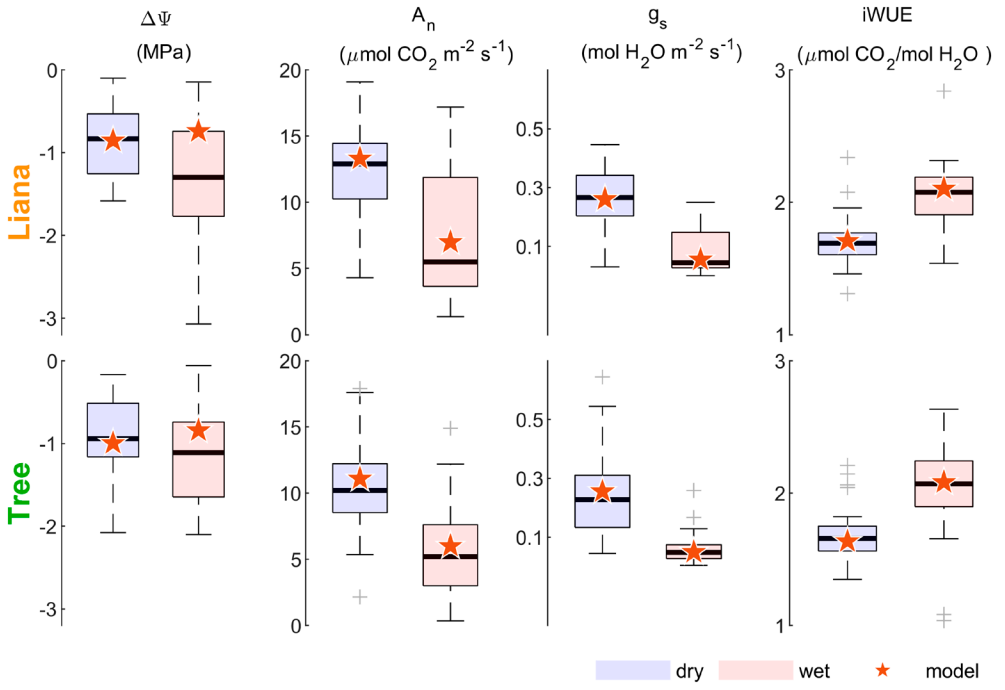

Fig. 6. Model benchmarking to physiological trait data for lianas and trees measured during wet and dry season by Smith-Martin et al., (36), Parque Municipal Summit, Panama). Model results (★) are obtained for the in situ measurement conditions (i.e., I_0: 1,200 μmol m^{-2} s^{-1}; T_C: 32 °C; VPD:0.6 and 1.7 MPa for wet and dry, resp.; and soil water potential = in situ predawn water potentials). ΔΨ is the plants' water potential gradient (i.e., midday–predawn water potential), A_N the net photosynthetic rate, g_S the stomatal conductance, and iWUE the water use efficiency. Optimized traits are the cost of water (c_0), the whole plant hydraulic conductance per leaf area (K), and the maximum carboxylation velocity at 25 °C reference temperature (V_{cmax}). The boxplots' central bar, and *Bottom* and *Top* edges show the median and 25th and 75th percentiles. Outliers are shown as +.

long-term, geographically widespread surveys of lianas and trees to facilitate dynamic hypothesis testing. Also critical are experimental studies that simulate environmental changes, like drought, and terrestrial 3D laser scanners (i.e., LIDAR; 'Laser Imaging, Detection, And Ranging') can improve quantification of liana canopy occupancy and provide detailed forest structure and liana impact assessments (60, 61). Contemporarily, the characterization of liana rooting and water uptake strategies, which are currently little explored, presents another promising research direction for model development and understanding tree–liana interactions (11, 31, 62–64). Finally, because lianas show interspecific variability in physiological traits and growth strategies (65, 66), different liana species may vary in their response to environmental changes. Therefore, the study and implementation of such heterogeneity among lianas could further aid our understanding of ecosystem dynamics in a changing world.

Material and Methods

This study theoretically investigates how altered environmental conditions that impact forest productivity (e.g., elevated CO_2 and increasing drought) and their associated changes in tree and liana performance (e.g., in vital rates) may drive liana proliferation. We use the forest of Barro Colorado Island (BCI, Panama) as a testbed because of the availability of extensive datasets on trees and lianas and because a significant increase in lianas has been documented (12). To illustrate the proposed conceptual framework (Fig. 1), we study the impact of increasing ambient CO_2 concentration ("CO_2 increase") and dry season length ("Drought shift") on growth rates, and how these changes impact the liana prevalence in the forest canopy (P_L).

Model Framework. We define a mechanistic forest model consisting of three distinct components (Fig. 1): i) a physiological model which derives optimal net carbon gain (G^*) for a given set of environmental conditions, ii) a plant allocation model which allocates G^* to growth and fecundity rates from growth form-specific allometry and allocation strategies, and iii) a size-structured host-parasite demographic model which allows evaluating how differential physiological/growth responses of lianas and trees translate into liana canopy prevalence, representing a proxy for the competitive fitness of lianas. The three components operate at different spatial and temporal scales: the physiological model is computed at high temporal timescales, allowing instantaneous calculations of a single plant's photosynthetic rates for fluctuating environmental conditions (diurnal and seasonal). The rates are then integrated at the annual time step and parsed into the plant allocation model. The demographic model represents the growth, mortality, and interactions among plants. It operates at a time scale beyond the life of a single plant.

A short description of the models' key equations, assumptions, and parameterization is provided below. For a complete overview of variables, definitions, and units, and a more extensive description of the model equations, we refer to appendices B through E. Similarly, we restrict the section on model parameterization and benchmarking to a synopsis, with an extensive description of the datasets used, model parameterization, calibration, and sensitivity provided in Appendices F and G. The model is implemented in Matlab (The Math Works, Inc., version R2020b), and is accessible via GitHub "HannesDeDeurwaerder/LianaModel."

Physiological Model. In this section, we derive instantaneous rates of carbon gain for a sun-exposed leaf using a coupled leaf biochemical and plant hydraulic model as a function of a set of plant traits and environmental conditions The carbon gain, G, is defined as the difference between the instantaneous rate of net photosynthesis, A_N, and the cost of water stress, C_w, such as drought-induced embolisms and cell dehydration that can diminish plants' hydraulic conductivity and consequently adversely impact their ability to sequester carbon (67). To reduce tension on the xylem that could cause irreparable damage or costs to repair and rebuild compromised tissues (e.g., refill embolized vessels), plants actively control the stomatal aperture (68–70). The leaf biochemical model is based on the Michaelis–Menten type dependence upon intercellular CO_2 concentration (71), and a stomatal conductance optimization scheme to link the internal to the ambient CO_2 concentration, c_a.

Water moves along the plant driven by a water potential gradient, according to Darcy's law, and it is directly influenced by the average soil water potential in contact with the root system ($\tilde{\psi}_s$) and atmospheric evaporative demand through vapor pressure deficit (D). The plant is represented as a three-element hydraulic system (adapted from refs. 72 and 73), exemplifying water uptake and transport through absorbing roots, transporting organs (xylem tissue in stem, branches, and petioles), and the evaporative surface of the leaves.

The vulnerability of the hydraulic system to water stress is expressed by the loss of conductivity, i.e. the decline of plant conductance as water potential becomes more negative in the xylem, increasing the resistance to water transport. The maximum conductance of each organ (root, stem, and leaves) and the water potential corresponding to a loss of 50% in conductivity are important plant traits that determine the hydraulic behavior of a plant. Importantly, our model assumes a "perfect recovery" of the hydraulic conductance once the conditions that induced the water stress cease and water potential increases.

However, the water stress has a cost for the plant. This cost is assumed to be nonlinearly related to leaf water potential, ψ_L, in line with theoretical and empirical insights suggesting a concave upward pattern (69, 70):

$$C_w = c_0 \left(\frac{\psi_L}{\pi_{tlp}} \right)^2, \quad [5]$$

were c_0 is the cost parameter for water stress, and the ratio between ψ_L and the leaf water potential at the turgor loss point, π_{tlp}, represents a proxy for the safety margin of hydraulic risk.

By assuming a well-coupled leaf, i.e., $E = g_s D$, where E and g_s are plant transpiration and stomatal conductance, respectively, we can express G as a nonlinear function of g_s, which can be optimized numerically. Specifically, given a set of environmental conditions $\boldsymbol{\theta} = [c_a, D, PAR, T_{air}, \tilde{\psi}_s]$ and growth-form-specific photosynthetic and hydraulic traits $\boldsymbol{\lambda} = [V_{cmax}, J_{max}, K_{max}, p_{50}, c_0]$, the stomatal conductance optimization can be formulated as

$$G^*(g_s^* | \boldsymbol{\theta}, \boldsymbol{\lambda}) = max_{g_s} \; G(g_s, \boldsymbol{\theta}, \boldsymbol{\lambda}). \quad [6]$$

With PAR the photoactive incoming radiation, T_{air} the ambient air temperature, J_{max} the maximum electron transport rate, K_{max} the maximum hydraulic conductance, p_{50} the water potential corresponding to a 50% loss in whole plant conductance, and V_{cmax} the maximum carboxylation velocity. Our analysis evaluates the physiological model separately for wet and dry seasons. The annual carbon gain is computed by summing wet and dry season daily budgets for different lengths of the dry season.

Plant Allocation Model. We express the plant's structural biomass increases, dB/dt, and plant's reproduction, F, as proportional to canopy size, a_C, times the available carbon per unit of crown area (net photosynthesis minus carbon cost for water stress; see above), after deducting leaf/root respiratory demands and tissues turnover and allocation to reproduction:

$$\eta \frac{dB}{dt} = (1 - \varphi)(\underbrace{\bar{A}_n - \bar{C}_w}_{\bar{G}_*} - \bar{C}_m) a_C, \quad [7a]$$

$$F = \frac{\varphi}{\eta} (\bar{A}_n - \bar{C}_w - \bar{C}_m), \quad [7b]$$

where η presents the costs of biomass construction, but it can also include costs for nutrient acquisition (e.g., biological nitrogen fixation) and NSC storage [assumed proportional to biomass (74)]. φ is the fractions of available carbon allocated to reproduction, and C_m the maintenance cost which incorporates root respiration and tissue turnover per unit of crown area (leaf respiration is already accounted for in A_n). The overbar denotes annual averages. For a complete formulation of the plant carbon budget, see ref. 73.

By using power-law allometric equations linking canopy size a_C to structural biomass, B, i.e., $B = \phi a_C^{\theta}$, we can solve (Eq. **7a**) and compute the growth rate, g associated with the plant dimension that grows linearly with time, $x = \frac{1}{\phi} \frac{B}{a_C}$ as:

$$g = \frac{\theta - 1}{\theta} \frac{1 - \varphi}{\eta \phi} \left(\bar{G}^* - \bar{G}_0^* \right). \quad [8]$$

The plant dimension x is related to diameter by $x \propto D^{c(\theta-1)}$, where θ and c are the scaling exponents of biomass and crown area allometries, i.e., $B \propto D^{c\theta}$ and $a_c \propto D^c$

Finally, to aid model simulations and interpretation, we express g and F to the current conditions (subscript 0).

$$g = g_0 + \frac{\theta - 1}{\theta} \frac{1 - \varphi}{\eta \phi} \left(\bar{G}^* - \bar{G}_0^* \right), \quad [9a]$$

$$F = F_0 + \frac{\varphi}{\eta} (\bar{G}^* - \bar{G}_0^*). \quad [9b]$$

Host-Parasite Demographic Model. The demographic host-parasite model considers three distinct demographic tree cohorts: understory trees, and sun-exposed canopy trees, which are either liana-free or liana-infested. The model uses the so-called perfect plasticity approximation (PPA) to simplify plant competition for light under the assumption that crown growth is sufficiently plastic and crowns have relatively flat tops (75). According to the PPA, a fixed-size threshold, x_*, separates the overstory from the understory and it is determined when the sum of the canopy area of all individuals above the threshold equals the forest ground area.

The forest dynamics are represented by a system of von Foerster partial differential equations along the size x, which is the dimension in which trees grow linearly with time (see above). Specifically, trees grow in the understory up to x_* (i.e., $x < x_*$) and, subsequently, transition into the cohort of canopy trees when $x \geq x_*$. Once in the canopy, trees may become infested by lianas, in which case they stop growing. Lianas infest only canopy trees as they need light to proliferate, though understory trees can serve as platforms to reach the canopy level. The following equations represent these dynamics for the understory (N_u), liana-free canopy (N_c), and infested canopy trees (N_i), respectively:

$$\frac{dN_u}{dt} = -g_u \frac{dN_u}{dx} - \mu_u N_u \quad g_u N_u(x_0) = R_T \quad x < x_*, \quad [10a]$$

$$\frac{dN_c}{dt} = -g_c \frac{dN_c}{dx} - (\mu_c + \lambda(x, x_*)) N_c + \xi N_i \quad (g_c - g_*) N_c(x_*) = (g_u - g_*) N_u(x_*) \quad x \geq x_*, \quad [10b]$$

$$\frac{dN_i}{dt} = \lambda(x) N_c - (\mu_c + \upsilon + \xi) N_i \quad x \geq x_*, \quad [10c]$$

where μ and g are the mortality and growth rates, $\lambda(x, x_*)$ is the size-dependent liana infestation force (see below), υ the liana-induced lethality, and ξ the liana shedding rate, which comprises active shedding of liana via branch abscission (23) and liana mortality sensu lato, both contributing to a reduction in the liana occupancy in the host. R_T is the tree recruitment rate.

Liana infestation starts on the forest floor, where juvenile lianas or clonal tillers locate potential host stems, which they subsequently climb in dark or partial light (76). Thus, the probability of a liana emerging from the understory layer and reaching the hosts' canopy, pc, is crucial to the model because many will fail or die before reaching the canopy. We assume that emerging from the understory is the most arduous stage for lianas, so we neglect the remaining time a liana takes to reach a host crown (i.e., $p_c = p_c(x_*)$; unless otherwise specified). The arrival of a liana at the top of its host can thus be regarded as a Poisson process with a specific rate determined by the product of the number of juvenile lianas or clonal tillers scavenging the forest floor and the host stem density, as in classic Lotka–Volterra host-parasite models (77). When a liana reaches the top of its host, it expands its crown according to the liana allometric growth rate (g_L) until the tree crown is completely covered. Multiple lianas with different arrival times may infest a single host. This allows expressing the infestation force $\lambda(x, x_*)$ as a function of host size:

$$\lambda(x, x_*)^{-1} = \frac{1}{g_L} \log \left(\frac{\left(\frac{x}{x_{*,L}} \right)^{\frac{1}{\theta - 1}}}{g_L R_L p_c(x_*)} - 1 \right), \quad [11]$$

where R_L is the lianas recruitment rate, $x_{*,L}$ the initial liana size when arriving at the host's canopy (see *SI Appendix, Appendix E* for details and derivation).

We assume that only noninfested canopy and infested canopy trees contribute to the reproduction of tree and liana, respectively. Finally, the system (11) is solved at equilibrium with the conditions that the product of the fecundity rates per unit of crown area and their canopy occupancies equal their recruitment rates:

$$R_T = n_T F_T P_T, \quad [12a]$$

$$R_L = n_L F_L P_L, \quad [12b]$$

where n_j converts the amount of carbon into the number of recruits, and the canopy occupancies are computed as

$$P_T = \int_{x_*}^{\infty} N_c(x) x^{\frac{1}{\theta-1}} dx, \quad [\mathbf{13a}]$$

$$P_L = \int_{x_*}^{\infty} N_l(x) x^{\frac{1}{\theta-1}} dx. \quad [\mathbf{13b}]$$

By defining $P_T + P_L = 1$, we obtain a closed system of integral equations for the unknown variables x_*, R_L, and R_T.

Model Parameterization and Benchmarking. The model was parameterized and calibrated to represent generic lianas and trees at BCI, briefly discussed here, but detailed in *SI Appendix, Appendix F*. Physiological parameters for each growth form are obtained from previous studies, following the priority cue of being conducted in BCI, in nearby forests in the Panamanian Isthmus, or compiled from existing literature elsewhere (*SI Appendix, Appendix B*). The biomass allometric equations for lianas and trees are adapted from Schnitzer et al. (78) and Martínez Cano et al. (79), respectively. The canopy allometric equations for trees follow Martínez Cano et al. (79). A BCI-specific liana canopy allometry was obtained from the liana census data (12), as is detailed in *SI Appendix, Appendix F*. The environmental drivers are obtained from a microclimatic tower located on the top plateau of BCI during the period 2016 to 2019 and collected at 5 min time step [see Detto and Pacala (73) for details]. Data were divided into wet and dry seasons based on soil moisture conditions and rainfall. Average diurnal patterns were computed for each season (*SI Appendix, Appendix F*) and used to upscale the instantaneous carbon gain to a yearly value for a given fraction of dry season days, Q, (current conditions: Q = 1/3).

Demographic data used for parameterizing and benchmarking the demographic model were obtained from the BCI 50 ha forest dynamic plot (27) and from two censuses of lianas (12) conducted on the same plot in 2007 and 2017. These data were used to compute current conditions' vital rates (mortality and growth rates) and the threshold size that separates the understory from the canopy, $D_* = 33$ cm (*SI Appendix, Appendix F*).

The tree census data were also used to compute the size abundance distribution of canopy trees and compare it with simulations of current BCI conditions. The liana canopy occupancy as a function of host size for BCI were obtained from ground-level observation by Visser et al., (53). Subsequent calculated of current liana canopy prevalence for BCI using this function ($P_L = 20\%$.) was consistent with the airborne hyperspectral-monitoring study at the nearby Gigante site by Marvin et al. (54) (*SI Appendix, Appendix F*).

The physiological model was benchmarked to various empirically obtained physiological traits for lianas and trees measured during wet and dry seasons (Parque Municipal Summit, Panama) (Fig. 6) (36). Specifically, model results produced for the corresponding in situ measurement conditions and compared to the physiological trait median while simultaneously optimizing the cost for water (c_0), the maximum whole plant hydraulic conductance per leaf area (K_{max}), and the maximum carboxylation velocity at 25 °C reference temperature (V_{cmax25}) for both lianas and trees. The benchmarking physiological traits were g_s, A_N, iWUE (i.e., A_N/g_s), and the total water potential gradient ($\Delta\psi$; i.e., midday-predawn water potential), for which the optimization minimized the accumulated weighted difference between simulated, $x_{mod,i}$, and observed, $\bar{x}_{obs,i}$, traits $\left(\min\left(\sum_{i=1}^{n} \left|x_{mod,i}/\bar{x}_{obs,i} - 1\right|\right)\right)$. Environmental conditions were set at I_0 =1,200 μmol m^{-2} s^{-1}, T_c =32 °C, and Ψ_s = measured in situ predawn water potentials. Vapor pressure deficit for wet and dry seasons were set at 0.6 and 1.7 MPa.

The calibration of the allometric growth model required G^* from the physiological model run under standard conditions to generate average growth rates measured in the BCI liana and tree censuses. Here, the flux tower–obtained gross primary productivity data was used as a quantitative validation of simulated G^*. Next, yearly growth rate increases corresponding to a known productivity change as observed by the flux tower were extracted from the census data, and subsequently used to benchmark simulated growth rates under a similar productivity change by calibrating η. Finally, the parameters $n_L F_L$ and $n_T F_T$ (Eq. **12**) were benchmarked so that the demographic model outputs for liana canopy occupancy, P_L, and x_* (or equivalent D_*) met representative values for BCI ($P_L = 20\%$, and $D_* =$ 33 cm, respectively).

The sensitivity targeted validation of each modules' responses to random assignment of critical liana parameters within a ±5% variability range of their standard values (see *SI Appendix*, Table S1; Latin hypercube sampling; 25,000 iterations per module). Simulation outputs were normalized to the output of the standard run to assess the relative deviation. More details and figures are provided in *SI Appendix, Appendix G*.

Analysis.

Forest structural properties. We implemented multiple liana infestation algorithms (Table 1) which are modifications of Eq. **11**, but differ in their combination and characterization of made assumption: First, i) the probability of lianas to emerge from the understory layer, p_c, can be set proportional to the height of the canopy layer, $p_c(x_*)$, or to the size of the climbed host, $p_c(X)$. The former assumes that when a climbing liana reaches the transition between understory and canopy layer, it immediately experiences optimal light and growing conditions, resulting in a negligible remaining time to reach the host crown. The alternative assumes that lianas always climb in light-limited conditions until the host size is reached. Second, ii) the initial crown size of a liana arriving at their hosts' canopy, $x_{*,l}$, can be ignored ($x_{*,l} = 0$) or considered from the liana growth allometry. Finally, iii) the liana crown expansion rate can follow a power-law or exponential rate. The latter is an interesting case where we assume lianas to be a perfectly hydraulic-constrained organism that must double its biomass to double its crown area. We implemented all possible liana infestation algorithms constructed as a combination of the above assumption, evaluated their performance against observed fractions of liana-occupied canopy area at BCI at the level of individual trees (COI), and at plot level (P_L, liana prevalence). The algorithm considering $p_c(x_*)$, $x_{*,l} \neq 0$, and $\lambda_{exponential}$ provided the best data fit (Model 1, Fig. 3), and was considered for all other analyses.

Additionally, two distinct conceptual host-infestation schemes were implemented and compared. A *single liana infestation scheme* assumes that each host can be infested by only one liana. When the infesting liana fully covers its host, the liana stops investing in growth and allocates all net carbon gain into reproduction (i.e., $\varphi = 1$). The *multiple liana infestation scheme* allows for multiple lianas to infest a single host. These infesting lianas will follow a PPA-like approach filling up the entire hosts' canopy, upon which they start competing for canopy space. Trying to overshade one another requires continued investment in growth, implying the continuation of the standard growth strategy with a constant fraction of carbon gained allocated to growth. Qualitatively and quantitatively, both conceptual host-infestation schemes gave similar results, so we limit our analysis to the latter because of its higher realism to field observations of multiple liana infestations.

Case study: Equilibrium conditions. The overall Neotropical forest productivity is increasing, a phenomenon attributed to secular changes in local climate, ambient CO_2 concentration, or nutrient conditions (80–84). Differences in growth responses of lianas and trees associated with such productivity increases may have instigated the observed liana proliferation (1, 31). The physiological module in our model framework accommodates such growth responses to shifts in environmental conditions, manifesting growth-form-specific G^* and responses herein. Note that "current conditions" correspond to a liana canopy prevalence of 20%, a forest structure where $D_* = 33$ cm, and a CO_2 concentration of 400 ppm. We study the impact of an increase in ambient CO_2 concentration (c_a: 400 → 425 ppm; scenario CO_2 increase) and in dry season length (Q: 123 → 136 d; scenario Drought shift) on liana prevalence and in overall tree biomass. The latter is derived by using the average wood density for trees in the BCI 50 ha plot (i.e., 0.2065 g cm^{-3}) and the model provided tree abundance distribution. As a second layer in our analysis, we altered the relative growth response sensitivity to an increase in CO_2 for lianas and trees from its baseline value, i.e., $\beta_L = \beta_T = 1$ (obtained from ref. 85), such that all potential scenarios depicted in the conceptual framework (Fig. 1) emerge from the model. For all analyses, we present the resulting growth rates for a canopy liana and tree with respective stem diameters of 1.6 and 33 cm (i.e., corresponds to standard D_* for lianas and trees at BCI).

Case study: Transient dynamics. The study of stable states assesses the long-term state of the forest in response to a change in environmental conditions, assuming the forest distribution and dynamics to be in equilibrium with the climate conditions it is subjected to (86, 87). In reality, the rate of change may outpace a forest's ability to remain in dynamic equilibrium which may instigate complex transient dynamics (88). At short time scales, temporary yet

Table 1. Distinct liana infestation algorithm assumptions and definitions of those visualized in Fig. 3

Probability of a liana to emerge from the understory layer (p_c)

p_c set proportional to the height of the canopy layer, x_*, neglecting the remaining time for a liana to reach a host crown.	p_c set proportional to the height of its host.
$p_c(x_*) = e^{-\frac{\mu_{u,L}}{g_{u,L}}\left(\frac{\vartheta_T}{\vartheta_L}\right)^{1/\gamma} x_*}$	$p_c(x) = e^{-\frac{\mu_{u,L}}{g_{u,L}}\left(\frac{\vartheta_T}{\vartheta_L}\right)^{1/\gamma} x}$

Initial liana size when arriving at hosts' canopy ($x_{*,l}$)

Lianas arrive at the hosts' canopy with no initial size.	Lianas arrive at the hosts' canopy with an initial size proportional to x_* or the host size (x instead of x_*).
$x_{*,l} = 0$	$x_{*,l} = \left[\left(\frac{\vartheta_T}{\vartheta_L}\right)^{1/\gamma} x_*\right]^{\frac{1}{\theta-1}}$

Liana infestation force (λ)

Power-law	Exponential
$\lambda = g_L\left[\left(\frac{\theta}{\theta-1}\frac{g_L x^{\frac{1}{\theta-1}}}{R_L p_c} + x_{*,l}^{\frac{\theta}{\theta-1}}\right)^{\frac{\theta-1}{\theta}} - x_{*,l}\right]^{-1}$	$\lambda = g_L\left[log\left(\frac{\left(\frac{x}{x_{*,l}}\right)^{\frac{1}{\theta-1}}}{g_L R_L p_c} - 1\right)\right]^{-1}$

Conceptual infestation algorithms visualized in Fig. 3

Model 1 (standard)	Model 2	Model 3
This conceptual infestation algorithm provided the best fit for the observed data in BCI.	This conceptual infestation algorithm resembles a scenario where it becomes exponentially more difficult to successfully infest with increasing host size.	This conceptual infestation algorithm resembles a scenario where infestation success is as good as independent of host size.
$\lambda = g_L\left[log\left(\frac{\left(\frac{x}{x_{*,l}}\right)^{\frac{1}{\theta-1}}}{g_L R_L p_c(x_*)} - 1\right)\right]^{-1}$	$\lambda = g_L\left[\left(\frac{\theta}{\theta-1}\frac{g_L x^{\frac{1}{\theta-1}}}{R_L p_c(x)}\right)^{\frac{\theta-1}{\theta}}\right]^{-1}$	$\lambda = g_L\left[log\left(\frac{\left(\frac{x}{x_{*,l}}\right)^{\frac{1}{\theta-1}}}{R_L p_c(x_*)}\right)\right]^{-1}$

A parameter description is provided below, with more details available in *SI Appendix, Appendix B*. With p_c the probability of a liana reaching the canopy layer and hosts' canopy; $\mu_{u,l}$ the mortality rate of understory liana; $g_{u,l}$ the growth rate of understory liana (in the x-dimension); ϑ_l and ϑ_T the Liana and Tree height allometric factor, respectively; γ the tree and liana height allometric exponent, set at 0.5; $x_{*,l}$ the initial liana size when arriving at the host's canopy; x_*^T the minimal x-dimensional tree size for an individual to be in the canopy layer; θ the canopy size allometric exponent in the x-dimension; λ the liana crown expansion rate; g_L the growth rate of a canopy liana (in the x-dimension); R_L The recruitment rate of the parasite, i.e., the number of lianas reaching a tree crown per unit of time.

quantitative perturbations deviating from the expected trends may emerge from differences in response times between organisms, a phenomenon that ultimately could lead to alternative stable states and regime shifts (33, 34). Consequently, this motivates a transient dynamical analysis for which we simulate the effect of a 50-y-long stepwise increase in ambient CO_2 concentration (c_a: 330 → 425 ppm, corresponding to the observed range from 1975 to 2024 A.D.) on liana prevalence and forest structure. Here, we impose a liana relative growth response sensitivity to an increase in CO_2 for which the experienced CO_2 increase does not lead to an increase in liana prevalence in equilibrium conditions ($\beta_L = 0.41$). In other words, we pursue a condition where the positive impact of the increase in CO_2 on the lianas' infestation force is perfectly balanced by the negative impact they experience from the concurrent increasing forest structure.

Data, Materials, and Software Availability. The MATLAB implementation of both the model and analyses are available in the GitHub repository HannesDeDeurwaerder/LianaModel. The 50-ha tree census and the eddy covariance data for Barro Colorado Island (Panama), and the benchmarking dataset of Smith-Martin et al. (36) are all accessible via the DRYAD repository (https://doi.org/10.15146/5xcp-0d46; https://doi.org/10.5061/dryad.3tx95x6j5; and https://doi.org/10.5061/dryad.844rs7d, respectively). For the availability of the liana census and COI data, readers are referred to refs. 12 and 53 respectively.

ACKNOWLEDGMENTS. This research was funded by the Carbon Mitigation Initiative at Princeton University (H.P.T.D.D. and M.D.), the CML Impact fund at Leiden University (M.D.V.), and the Belgian American Educational Foundation (BAEF to H.P.T.D.D.). We are grateful to the editors and anonymous reviewers for their comments, and Cora N. Betsinger for proofreading of this manuscript.

Author affiliations: [a]Department of Ecology and Evolutionary Biology, Princeton University, Princeton, NJ 08544; [b]Smithsonian Tropical Research Institute, Balboa 0843-03092, Panama; [c]Institute of Environmental Sciences (CML), Leiden University, Leiden CC 2333, The Netherlands; and [d]Department of Biological Sciences, Marquette University, Milwaukee, WI 53201

1. O. L. Phillips *et al.*, Increasing dominance of large lianas in Amazonian forests. *Nature* **418**, 770–774 (2002).
2. S. J. Wright, Tropical forests in a changing environment. *Trends Ecol. Evol.* **20**, 553–560 (2005).
3. S. M. Durán, E. Gianoli, Carbon stocks in tropical forests decrease with liana density. *Biol. Lett.* **9**, 20130301 (2013).
4. L. L. Ingwell, S. Joseph Wright, K. K. Becklund, S. P. Hubbell, S. A. Schnitzer, The impact of lianas on 10 years of tree growth and mortality on Barro Colorado Island, Panama. *J. Ecol.* **98**, 879–887 (2010).
5. G. M. F. Van der Heijden, O. L. Phillips, Liana infestation impacts tree growth in a lowland tropical moist forest. *Biogeosciences* **6**, 2217–2226 (2009).
6. B. Tymen *et al.*, Evidence for arrested succession in a liana-infested Amazonian forest. *J. Ecol.* **104**, 149–159 (2016).
7. S. A. Schnitzer, F. Bongers, R. J. Burnham, F. E. Putz, *Ecology of Lianas* (WIley-Blackwell, 2015).
8. S. A. Schnitzer, F. Bongers, Increasing liana abundance and biomass in tropical forests: Emerging patterns and putative mechanisms. *Ecol. Lett.* **14**, 397–406 (2011).
9. A. L. S. Santiago, S. J. Wright, Leaf functional traits of tropical forest plants in relation to growth form. *Funct. Ecol.* **21**, 19–27 (2007).
10. T. P. Wyka, J. Oleksyn, P. Karolewski, S. A. Schnitzer, Phenotypic correlates of the lianescent growth form: A review. *Ann. Bot.* **112**, 1667–1681 (2013).

11. Y. J. Chen *et al.*, Water-use advantage for lianas over trees in tropical seasonal forests. *New Phytol.* **205**, 128–136 (2014).
12. S. A. Schnitzer *et al.*, Local canopy disturbance as an explanation for long-term increases in liana abundance. *Ecol. Lett.* **24**, 2635–2647 (2021).
13. F. E. Putz, The natural history of lianas on Barro Colorado Island, Panama. *Ecology* **65**, 1713–1724 (1984).
14. S. A. Schnitzer, J. W. Dalling, W. P. Carson, The impact of lianas on tree regeneration in tropical forest canopy gaps: Evidence for an alternative pathway of gap-phase regeneration. *J. Ecol.* **88**, 655–666 (2000).
15. R. A. Londré, S. A. Schnitzer, The distribution of lianas and their change in abundance in temperate forests over the past 45 years. *Ecology* **87**, 2973–2978 (2006).
16. W. F. Laurance *et al.*, Rain forest fragmentation and the structure of Amazonian liana communities. *Ecology* **82**, 105–116 (2001).
17. S. J. DeWalt *et al.*, Annual rainfall and seasonality predict pan-tropical patterns of liana density and basal area. *Biotropica* **42**, 309–317 (2010).
18. B. P. Kurzel, S. A. Schnitzer, W. P. Carson, Predicting liana crown location from stem diameter in three Panamanian lowland forests. *Biotropica* **38**, 262–266 (2006).
19. S. A. Schnitzer, Testing ecological theory with lianas. *New Phytol.* **220**, 366–380 (2018).
20. D. C. Marvin, K. Winter, R. J. Burnham, S. A. Schnitzer, No evidence that elevated CO2 gives tropical lianas an advantage over tropical trees. *Glob. Chang. Biol.* **21**, 2055–2069 (2015).
21. S. C. Pasquini, S. J. Wright, L. S. Santiago, M. Uriarte, Lianas always outperform tree seedlings regardless of soil nutrients: Results from a long-term fertilization experiment. *Ecology* **96**, 1866–1876 (2015).
22. D. C. Nepstad, I. M. Tohver, R. David, P. Moutinho, G. Cardinot, Mortality of large trees and lianas following experimental drought in an amazon forest. *Ecology* **88**, 2259–2269 (2007).
23. M. D. Visser *et al.*, A host–parasite model explains variation in liana infestation among co-occurring tree species. *J. Ecol.* **106**, 2435–2445 (2018).
24. H. C. Muller-Landau, S. W. Pacala, "What determines the abundance of Lianas and Vines?" in *Unsolved Problems in Ecology*, A. Dobson, D. Tilman, R. D. Holt, Eds. (Princeton University Press, 2020), pp. 239–264.
25. M. di Porcia *et al.*, Modeling the impact of liana infestation on the demography and carbon cycle of tropical forests. *Glob. Chang. Biol.* **25**, 3767–3780 (2019).
26. F. Meunier *et al.*, Unraveling the relative role of light and water competition between lianas and trees in tropical forests: A vegetation model analysis. *J. Ecol.* **109**, 519–540 (2021).
27. R. Condit *et al.*, Complete data from the Barro Colorado 50-ha plot: 423617 trees, 35 years. (2019). https://doi.org/10.15146/5xcp-0d46.
28. B. Gilbert, S. J. Wright, H. C. Muller-landau, K. Kitajima, Life history trade-offs in tropical trees and Lianas. *Ecology* **87**, 1281–1288 (2006).
29. M. Slot, K. Winter, In situ temperature response of photosynthesis of 42 tree and liana species in the canopy of two Panamanian lowland tropical forests with contrasting rainfall regimes. *New Phytol.* **214**, 1103–1117 (2017).
30. S. A. Schnitzer, S. Estrada-Villegas, S. J. Wright, The response of lianas to 20 yr of nutrient addition in a Panamanian forest. *Ecology* **101**, 1–9 (2020).
31. S. A. Schnitzer, A mechanistic explanation for global patterns of liana abundance and distribution. *Am. Nat.* **166**, 262–276 (2005).
32. S. Wang *et al.*, Lianas have a faster resource acquisition strategy than trees: Ground evidence from root traits, phylogeny and the root economics space. *J. Ecol.* **111**, 436–448 (2022).
33. D. Sahoo, G. Samanta, Oscillatory and transient dynamics of a slow–fast predator–prey system with fear and its carry-over effect. *Nonlinear Anal. Real World Appl.* **73**, 103888 (2023).
34. P. R. Chowdhury, S. Petrovskii, M. Banerjee, Oscillations and pattern formation in a slow-fast prey–predator system. *Bull. Math. Biol.* **83**, 1–41 (2021).
35. A. M. Willson, A. T. Trugman, J. S. Powers, C. M. Smith-martin, D. Medvigy, Climate and hydraulic traits interact to set thresholds for liana viability. *Nat. Commun.* **13**, 3332 (2022).
36. C. M. Smith-Martin *et al.*, Effects of dry-season irrigation on leaf physiology and biomass allocation in tropical lianas and trees. *Ecology* **100**, 1–12 (2019).
37. S. A. Schnitzer, G. M. F. van der Heijden, Lianas have a seasonal growth advantage over co-occurring trees. *Ecology* **100**, 1–30 (2019).
38. G. M. F. F. van der Heijden, J. S. Powers, S. A. Schnitzer, Effect of lianas on forest-level tree carbon accumulation does not differ between seasons: Results from a liana removal experiment in Panama. *J. Ecol.* **107**, 1890–1900 (2019).
39. U. G. Hacke, J. S. Sperry, J. K. Wheeler, L. Castro, Scaling of angiosperm xylem structure with safety and efficiency. *Tree Physiol.* **26**, 689–701 (2006).
40. S.-D. Zhu, K.-F. Cao, Hydraulic properties and photosynthetic rates in co-occurring lianas and trees in a seasonal tropical rainforest in southwestern China. *Plant Ecol.* **204**, 295–304 (2009).
41. M. T. van der Sande, L. Poorter, S. A. Schnitzer, L. Markesteijn, Are lianas more drought-tolerant than trees? A test for the role of hydraulic architecture and other stem and leaf traits *Oecologia* **172**, 961–972 (2013).
42. M. T. van der Sande, L. Poorter, S. A. Schnitzer, B. M. J. Engelbrecht, L. Markesteijn, The hydraulic efficiency–safety trade-off differs between lianas and trees. *Ecology* **100**, e02666 (2019).
43. F. E. Putz, H. A. Mooney, *The Biology of Vines* (Cambridge University Press, 1991),10.5860/choice.30-0291.
44. C. Signori-Müller *et al.*, Non-structural carbohydrates mediate seasonal water stress across Amazon forests. *Nat. Commun.* **12**, 1–9 (2021).
45. I. Maréchaux, M. K. Bartlett, A. Iribar, L. Sack, J. Chave, Stronger seasonal adjustment in leaf turgor loss point in lianas than trees in an Amazonian forest. *Biol. Lett.* **13**, 20160819 (2017).
46. C. R. Brodersen, T. Knipfer, A. J. McElrone, In vivo visualization of the final stages of xylem vessel refilling in grapevine (Vitis vinifera) stems. *New Phytol.* **217**, 117–126 (2018).
47. M. E. B. Sabot *et al.*, Predicting resilience through the lens of competing adjustments to vegetation function. *Plant Cell Environ.* **45**, 2744–2761 (2022).
48. S. Jones *et al.*, The impact of a simple representation of non-structural carbohydrates on the simulated response of tropical forests to drought. *Biogeosciences* **17**, 3589–3612 (2020).
49. R. Condit, Ecological implications of changes in drought patterns: Shifts in forest composition in Panama. *Potential Impacts Clim. Chang. Trop. For. Ecosyst.*, 273–287 (1998).
50. M. J. Campbell *et al.*, Edge disturbance drives liana abundance increase and alteration of liana–host tree interactions in tropical forest fragments. *Ecol. Evol.* **8**, 4237–4251 (2018).
51. S. J. Wright *et al.*, Long-term changes in liana loads and tree dynamics in a Malaysian forest. *Ecology* **96**, 2748–2757 (2015).
52. D. M. Newbery, C. Zahnd, Change in liana density over 30 years in a Bornean rain forest supports the escape hypothesis. *Ecosphere* **12**, e03537 (2021).
53. M. D. Visser *et al.*, Tree species vary widely in their tolerance for liana infestation: A case study of differential host response to generalist parasites. *J. Ecol.* **106**, 781–794 (2018).
54. D. C. Marvin, G. P. Asner, S. A. Schnitzer, Liana canopy cover mapped throughout a tropical forest with high-fidelity imaging spectroscopy. *Remote Sens. Environ.* **176**, 98–106 (2016).
55. F. E. Putz, D. M. Windsor, Liana phenology on Barro Colorado Island. *Biotropica* **19**, 334–341 (1987).
56. A. Gerardo, S. S. Mulkey, Seasonal changes in liana cover in the upper canopy of a neotropical dry. *Biotropica* **31**, 186–192 (1999).
57. J. A. Medina-Vega, S. J. Wright, F. Bongers, S. A. Schnitzer, F. J. Sterck, Vegetative phenologies of lianas and trees in two Neotropical forests with contrasting rainfall regimes. *New Phytol.* **235**, 457–471 (2022).
58. Z. Q. Cai, S. A. Schnitzer, B. Wen, Y. J. Chen, F. Bongers, Liana communities in three tropical forest types in Xishuangbanna, South-West China. *J. Trop. For. Sci.* **21**, 252–264 (2009).
59. T. Hölttä, H. Cochard, E. Nikinmaa, M. Mencuccini, Capacitive effect of cavitation in xylem conduits: Results from a dynamic model. *Plant Cell Environ.* **32**, 10–21 (2009).
60. S. M. K. Moorthy, K. Calders, M. di P. e Brugnera, S. A. Schnitzer, H. Verbeeck, Terrestrial laser scanning to detect liana impact on forest structure. *Remote Sens.* **10**, 1–19 (2018).
61. C. E. Waite *et al.*, Landscape-scale drivers of liana load across a Southeast Asian forest canopy differ to the Neotropics. *J. Ecol.* **111**, 77–89 (2022).
62. J. L. Andrade, F. C. Meinzer, G. Goldstein, S. A. Schnitzer, Water uptake and transport in lianas and co-occurring trees of a seasonally dry tropical forest. *Trees* **19**, 282–289 (2005).
63. C. M. Smith-Martin *et al.*, Allometric scaling laws linking biomass and rooting depth vary across ontogeny and functional groups in tropical dry forest lianas and trees. *New Phytol.* **226**, 714–726 (2020).
64. H. De Deurwaerder *et al.*, Liana and tree below-ground water competition-evidence for water resource partitioning during the dry season. *Tree Physiol.* **38**, 1071–1083 (2018).
65. K. Coppieters *et al.*, Two co-occurring liana species strongly differ in their hydraulic traits in a water-limited neotropical forest. *Front. For. Glob. Chang.* **5**, 836711 (2022).
66. F. Meunier *et al.*, Within-site variability of lianawood anatomical traits: A case study in laussat, French guiana. *Forests* **11**, 1–15 (2020).
67. M. H. Zimmermann, *Xylem Structure and the Ascent of Sap*, T. E. Timmel, Ed. (Springer, Berlin Heidelberg, ed. 1, 1983).
68. G. Katul, S. Manzoni, S. Palmroth, R. Oren, A stomatal optimization theory to describe the effects of atmospheric CO2 on leaf photosynthesis and transpiration. *Ann. Bot.* **105**, 431–442 (2010).
69. J. S. Sperry *et al.*, Pragmatic hydraulic theory predicts stomatal responses to climatic water deficits. *New Phytol.* **212**, 577–589 (2016).
70. A. Wolf, W. R. L. Anderegg, S. W. Pacala, Optimal stomatal behavior with competition for water and risk of hydraulic impairment. *Proc. Natl. Acad. Sci. U.S.A.* **113**, E7222–E7230 (2016).
71. G. D. Farquhar, S. von von Caemmerer, J. A. Berry, A biochemical model of photosynthetic CO_2 assimilation in leaves of C3 species. *Planta* **149**, 78–90 (1980).
72. J. S. Sperry, F. R. Adler, G. S. Campbell, J. P. Comstock, Limitation of plant water use by rhizosphere and xylem conductance: Results from a model. *Plant. Cell Environ.* **21**, 347–359 (1998).
73. M. Detto, S. W. Pacala, Plant hydraulics, stomatal control, and the response of a tropical forest to water stress over multiple temporal scales. *Glob. Chang. Biol.* **28**, 4359–4376 (2022).
74. M. E. Furze *et al.*, Whole-tree nonstructural carbohydrate storage and seasonal dynamics in five temperate species. *New Phytol.* **221**, 1466–1477 (2019).
75. N. Strigul *et al.*, Scaling from trees to forests: Tractable macroscopic equations for forest dynamics. *Ecol. Monographs* **78**, 523–545 (2008).
76. F. E. Putz, N. M. Holbrook, "Biomechanical studies of vines" in *The Biology of Vines*, F. E. Putz, H. A. Mooney, Eds. (Cambridge University Press, 1991), pp. 73–97.
77. C. J. Briggs, M. F. Hoopes, Stabilizing effects in spatial parasitoid-host and predator-prey models: A review. *Theor. Popul. Biol.* **65**, 299–315 (2004).
78. S. A. Schnitzer, S. J. DeWalt, J. Chave, Censusing and measuring lianas: A quantitative comparison of the common methods. *Biotropica* **38**, 581–591 (2006).
79. I. Martínez Cano, H. C. Muller-Landau, S. Joseph Wright, S. A. Bohlman, S. W. Pacala, Tropical tree height and crown allometries for the Barro Colorado Nature Monument, Panama: A comparison of alternative hierarchical models incorporating interspecific variation in relation to life history traits. *Biogeosciences* **16**, 847–862 (2019).
80. O. L. Phillips *et al.*, Changes in the carbon balance of tropical forests: Evidence from long- term plots. *Science* **282**, 439–442 (1998).
81. T. R. Baker *et al.*, Variation in wood density determines spatial patterns in Amazonian forest biomass. *Glob. Chang. Biol.* **10**, 545–562 (2004).
82. G. B. Bonan, Forests and climate change: Forcings, feedbacks, and the climate benefits of forests. *Science* **320**, 1444–1449 (2008).
83. J. Chave *et al.*, Assessing evidence for a pervasive alteration in tropical tree communities. *PLoS Biol.* **6**, 0455–0462 (2008).
84. R. J. W. Brienen *et al.*, Long-term decline of the Amazon carbon sink. *Nature* **519**, 344–348 (2015).
85. R. J. Norby *et al.*, Informing models through empirical relationships between foliar phosphorus, nitrogen and photosynthesis across diverse woody species in tropical forests of Panama. *New Phytol.* **215**, 1425–1437 (2017).
86. T. Webb III, Is vegetation in equilibrium with climate? How to interpret late-Quaternary pollen data. *Vegetatio* **67**, 75–91 (1986).
87. I. C. Prentice, P. J. Bartlein, T. Webb, Vegetation and climate change in eastern North America since the last glacial maximum. *Ecology* **72**, 2038–2056 (1991).
88. C. I. Prentice, M. T. Sykes, W. Cramer, A simulation model for the transient effects of climate change on forest landscapes. *Ecol. Modell.* **65**, 51–70 (1993).